

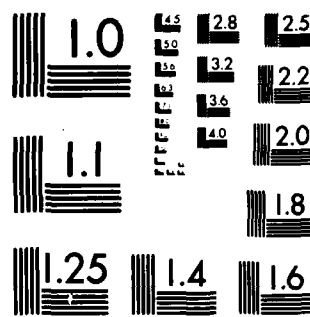
AD-A127 162 ESTIMATION OF THE CONCENTRATION OF A PHOTON-EMITTING
GAS IN AN EXTENDED SOURCE(U) DEFENCE RESEARCH
ESTABLISHMENT VALCARTIER (QUEBEC) S A BARTON MAR 83
UNCLASSIFIED DREV-4290/83

1/1

F/G 12/1

NL

END
DATE
FILED
5 83
DTIC



MICROCOPY RESOLUTION TEST CHART
NATIONAL BUREAU OF STANDARDS-1963-A

UNCLASSIFIED
UNLIMITED DISTRIBUTION

(3)

DREV REPORT 4290/83
FILE: 3633H-007
MARCH 1983

CRDV RAPPORT 4290/83
DOSSIER: 3633H-007
MARS 1983

AD A127162

ESTIMATION OF THE CONCENTRATION OF
A PHOTON-EMITTING GAS IN AN EXTENDED SOURCE

S.A. Barton

DTIC
SELECTED
APR 26 1983
S D

DMC FILE COPY

BUREAU - RECHERCHE ET DEVELOPPEMENT
MINISTÈRE DE LA DEFENSE NATIONALE
CANADA

Centre de Recherches pour la Défense
Defence Research Establishment
Valcartier, Québec

RESEARCH AND DEVELOPMENT BRANCH
DEPARTMENT OF NATIONAL DEFENCE
CANADA

NON CLASSIFIÉ
DIFFUSION ILLIMITÉE

33 04 22 002

DREV R-4290/83
FILE: 3633H-007

UNCLASSIFIED

CRDV R-4290/83
DOSSIER: 3633H-007

ESTIMATION OF THE CONCENTRATION OF
A PHOTON-EMITTING GAS IN AN
EXTENDED SOURCE

by
S.A. Barton

DTIC

ELECTED

APR 26 1983

H

CENTRE DE RECHERCHES POUR LA DEFENSE
DEFENCE RESEARCH ESTABLISHMENT
VALCARTIER
Tel: (418) 844-4271

Québec, Canada

March/mars 1983

NON CLASSIFIÉ

UNCLASSIFIED

1

ABSTRACT

Equations are derived, within the framework of geometrical optics, that relate the photon flux at a detector to the concentration of an emitting gas contained in an extended source of rectangular cross section, for two optical arrangements that have been used experimentally. Since the ratio of the experimental detector signals for the two quite dissimilar cases is in agreement with that predicted theoretically, the methods are validated.

A method is described for maximizing the signal at the detector, using a given lens, which may be applied to an extended source of general cross section.

RÉSUMÉ

Selon l'optique géométrique, on a dérivé des équations qui relient le flux de photons atteignant un détecteur à la concentration d'un gaz émettant dans une source étendue dont la coupe transversale est rectangulaire. Deux arrangements optiques sont considérés. Puisque le rapport des signaux expérimentaux pour ces deux cas tout à fait différents est en accord avec celui prédit théoriquement, les méthodes sont validées.

Une méthode est décrite afin de maximiser le signal d'un détecteur, pour une lentille donnée. Cette méthode peut être appliquée dans le cas d'une source étendue ayant une coupe transversale arbitraire.

Accession For	
NTIS ORG&I	
DTIC T/S	
Unclassified	
Justification	
By	
Distribution/	
Availability Codes	
Dist	Avail and/or Special
A	



UNCLASSIFIED

iii

TABLE OF CONTENTS

ABSTRACT/RÉSUMÉ	1
1.0 INTRODUCTION	1
2.0 LENS CASE	3
2.1 The General Contributing Object-Plane Radius	5
2.2 Light Cone Radius at any Position on the Image Side of the Lens	7
2.3 Object and Image Space Cross Sections	9
2.4 Fraction Intercepted by a Circular Detector	10
2.5 Fraction of Emitted Light Arriving at the Lens	13
2.6 Relation Between Emitting Gas Concentration and Photon Flux at a Detector	15
2.7 Calculation of the Lens Integral: A Numerical Example .	16
2.8 Choice of \bar{v} and s : Maximization of I_L	17
3.0 TUBE CASE	20
3.1 First Approximation: Detector Wholly Illuminated . . .	22
3.2 Inclusion of Boundary Region	24
3.3 Calculation of the Tube Integral: A Numerical Example .	28
4.0 LENS/TUBE RATIO: THEORY AND EXPERIMENT	30
5.0 CONCLUSIONS	34
6.0 ACKNOWLEDGEMENTS	34
7.0 REFERENCES	35
TABLES I to III	
FIGURES 1 to 12	
APPENDIX A - Fractional Area of a Circular Detector Illuminated Through a Cylindrical Tube by a Radiating Off-Axis Molecule	36

UNCLASSIFIED

1

1.0 INTRODUCTION

During continuing studies of a potential gas laser system it has been necessary to estimate the concentrations of several energetically excited molecules in a vacuum flow system. We have, for example, measured emissions from O_2 ($a^1\Delta g$) and NF ($b^1\Sigma^+_g$) in the near infrared ($1.27 \mu m$) and visible (529 nm) respectively. The spontaneous transition rates (k_g, s^{-1}) for these molecular states are both well established (1, 2), and so it is possible, in principle, to measure their concentrations passively in a gas flow using calibrated detectors and narrow-band interference filters. Typically, the detection system is arranged to view the active gases along an axis perpendicular to their flow, through a window of known transmittance. A lens is frequently used to increase the signal at the detector. The field of view of the detector then covers an extended source of variable cross section containing an emitting gas whose concentration is assumed constant. However, it would not be difficult to include the case of a gas whose concentration varies in a known way.

To calculate an accurate concentration, the volume of emitting gas that can contribute to the detector signal and the fraction of emitted light that arrives at the detector from any molecule in this contributing volume must be specified precisely.

This report is not intended to present an original theoretical treatment of the light-gathering properties of optical systems from extended sources. This has been dealt with elsewhere both in general terms (3, 4) and for the particular case of optimizing the focal length of a condensing lens to fill a spectrograph with light from a cylindrical extended source (5, 6).

This document is concerned with a somewhat different situation. It presents the methods that have been used to calculate accurately the photon flux at a detector under two optical arrangements employed to observe a particular source cavity that has a rectangular cross section. Either a circular convex lens or a cylindrical tube, which was blackened and baffled to minimize internal reflection, was placed between source and detector.

However, though a particular form of the extended source cross section is considered explicitly, the methods may be applied to any cross section. Also, the treatment of the lens case provides a general method for maximizing the signal at the detector, for a lens of a given focal length and diameter, from a completely general extended source.

As in previous work (5, 6), the geometrical optics approximation is made (diffraction effects are ignored).

Figure 1 defines the (left-handed) Cartesian coordinate system used in subsequent sections to describe the emitting gas. It also shows that the gas is constrained in the y-direction ($\pm c$) and in z (0 to L), but not in the x-direction. The field of view in x will thus be unconstrained.

Since the mathematical treatment of the two optical arrangements (lens and tube) is quite different, the theory may be verified by comparison with experiment: the ratio of experimental detector signals for the two situations (from identical gas flows) should agree with the calculated ratio of intensities at the detector. Thus it is not necessary to know absolute concentrations in order to verify the theory. When this has been validated, however, absolute concentrations can then be calculated with confidence from the equations given here for either case. Such concentration measurements have been made for excited oxygen and nitrogen fluoride, and will be presented in separate reports.

UNCLASSIFIED.

3

Results are given here (Chapter 4) for oxygen emission intensity ratios that show the agreement between theory and experiment to be within the measurement errors.

The final equations for gas concentration (Chapter 4) do not take into account any absorption of light by the emitting gas itself; i.e. self-absorption is neglected. They are therefore only valid for dilute gases, or transitions for which the probability is low, as in the cases of O_2 and NF that we have studied.

This work was performed at DREV between January and September 1982 under PCN 33H07, Research on Chemically Excited Lasers.

2.0 LENS CASE

This chapter describes a method for calculating the number of photons per second that arrive at a circular detector when a circular focusing lens is placed between it and the extended source shown in Fig. 1. Only thin lens formulae will be used.

The emitting volume will be treated as a continuum of contributing object planes (xy) to be mapped onto the detector plane. The fraction of each mapped surface intercepted by the detector will be derived. This, together with a function specifying the solid angle subtended to the lens by each point in the object plane, will be integrated through z-space to yield a total photon flux at the detector for a given gas concentration and emission rate.

Originally, the cylindrical symmetry imposed by the coaxial circular lens/detector arrangement will be exploited, the actual cavity dimensions being treated as constraints upon this.

UNCLASSIFIED

4

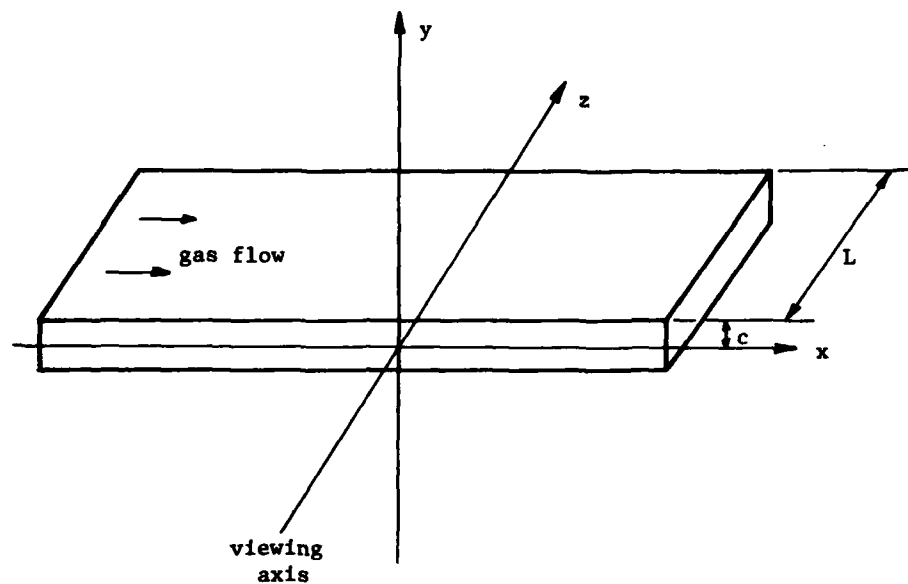


FIGURE 1 - Gas flow through a rectangular cavity

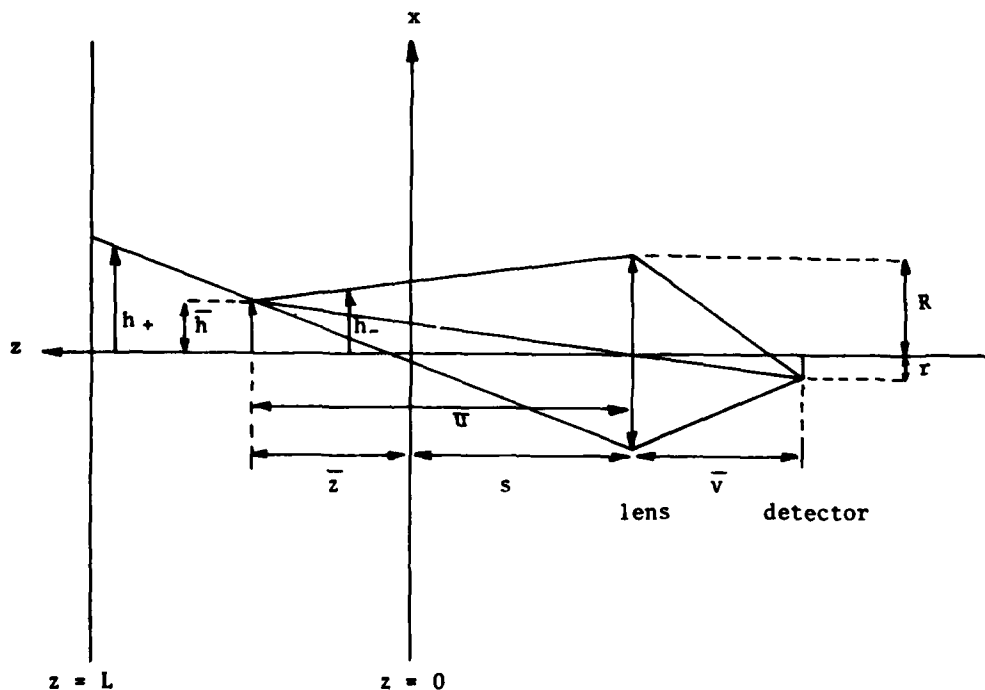


FIGURE 2 - Lens, detector and source in the xz-plane

2.1 The General Contributing Object-Plane Radius

Figure 2 shows a cross section through the xz plane of Fig. 1. A lens of focal length f and radius R is placed at a distance s from the window (at $z = 0$) of the extended source. The detector (radius r) is a distance \bar{v} from the lens. The bar above the v , as with other symbols used here, indicates a fixed parameter: \bar{v} is a particular value in the complete image space v .

There exists a \bar{u} (in the object space u) for a fixed (\bar{v}, s) configuration, such that an object of radius \bar{h} is mapped exactly into an image of radius r at the detector position. \bar{u} is given by

$$\bar{u} = \bar{f}\bar{v}/(\bar{v} - f) \quad [1]$$

provided $\bar{v} > f$, and \bar{u} lies between s and $s + L$.

The object radius, \bar{h} is

$$\bar{h} = \bar{u} \cdot r/\bar{v} \quad [2]$$

The general object position is

$$u(z) = z + s \quad [3]$$

with \bar{u} being a particular value $\bar{z} + s$.

At any other position on the z -axis ($z = 0, L$), the maximum object radius that can contribute to the intensity at the detector is given by $h+$ or $h-$ (see Fig. 2). This is because only rays passing through both \bar{h} and the lens can arrive at the detector. This is not to say that all rays leaving any $h(u)$ arrive at the detector, as we shall see.

So far, no way has been specified for choosing the lens and detector positions \bar{v} and s . Conventionally, the object position \bar{u} is required to be at the centre of the cavity ($\bar{z} = L/2$), and the object radius \bar{h} is chosen to be the cavity radius. Equations 1 and 2 are then implicitly simultaneous in two unknowns (\bar{v} , s). However, for the case considered here in which the source is unrestricted in the x -direction, \bar{h} is not clearly defined. For the moment, [1] and [2] simply define \bar{u} and \bar{h} for a given choice of \bar{v} and s .

It is necessary to have an expression for the general contributing object radius $h(u)$:

a) in $u < \bar{u}$, $h \equiv h-$ in Fig. 2 and the geometry gives:

$$(R - h-)/u = (R - \bar{h})/\bar{u} \quad [4]$$

using [2] yields:

$$h- = r.u/\bar{v} + R(\bar{u} - u)/\bar{u} \quad [5]$$

b) in $u > \bar{u}$, $h \equiv h+$

$$(R + h+)/u = (R + \bar{h})/\bar{u} \quad [6]$$

and similarly,

$$h+ = r.u/\bar{v} + R(u - \bar{u})/\bar{u}. \quad [7]$$

Thus in general, for $L + s > u > s$:

$$h(u) = r.u/\bar{v} + R|u - \bar{u}|/\bar{u} \quad [8]$$

Note that $h(\bar{u})$ reduces to \bar{h} (eq. 2) as required.

UNCLASSIFIED

7

$h(u)$ defines a continuum of objects that are radii of cross sections in the xy plane. Each of these objects will be focused, provided $s > f$, at a different position on the image side of the lens. Therefore it is necessary to know the radius of the circle at any point in the image space through which all rays from any object circle of radius $h(u)$ pass, so that the fraction of this light intercepted by the detector can be specified.

2.2 Light Cone Radius at any Position on the Image Side of the Lens

Consider Fig. 3. An object of radius h at u is focused at v with image radius i_0 . The radius of the cross section of the cone through which all light from the object passes is:

i^- at $v^- < v$, and
 i^+ at $v^+ > v$.

Now,

$$\tan\theta = (R - i_0)/v = (R - i^-)/v^- \quad [9]$$

so that

$$i^- = i_0 v^-/v + R(v - v^-)/v \quad [10]$$

Now consider the detector to be placed at v^- ; i.e. $v^- \equiv \bar{v}$.

With

$$i_0 = vh/u \quad [11]$$

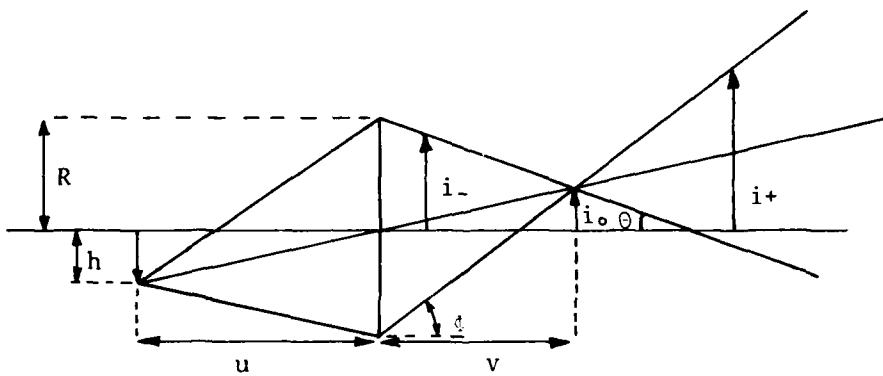


FIGURE 3 - Light cone radii on the image side of the lens

Eq. 10 becomes

$$i^- = \bar{h}\bar{v}/u + R(v - \bar{v})/v \quad [12]$$

for $\bar{v} < v$.

Similarly for $v^+ > v$

$$\tan\Phi = (R + i^+)/v^+ = (R + i_0)/v \quad [13]$$

which leads to

$$i^+ = \bar{h}\bar{v}/u + R(\bar{v} - v)/v \quad [14]$$

for $\bar{v} > v$.

Thus, at a fixed position \bar{v} (detector position), the radius of the circle of light from an object of radius h may be written in a general form, using [12] and [14] as a function of object position u only:

$$i(u) = h(u)\bar{v}/u + R|v - \bar{v}|/v \quad [15]$$

UNCLASSIFIED

9

where $h(u)$ is given by [8] for all u , and

$$v(u) = fu/(u-f) \quad [16]$$

Using [8] and [16], $i(u)$ can be written explicitly as a function of u :

$$i(u) = r + 2\bar{R}v \left| \frac{1}{\bar{u}} - \frac{1}{u} \right| \quad [17]$$

which may also be written in the useful form:

$$i(u) = \bar{h}v/u + \bar{R}v \left| \frac{1}{\bar{u}} - \frac{1}{u} \right| \quad [18]$$

2.3 Object and Image Space Cross Sections

Equation 8 for $h(u)$ defines a continuum of circular emitting cross sections, and [18] for $i(u)$ gives the circles into which these are mapped at the detector position \bar{v} . The y -direction constraint imposed by the cavity dimension $\pm c$, (see Fig. 1) can now be included.

The shaded region of Fig. 4 shows the constrained emitting cross section, whose area is:

$$A_o(z) = 2[h^2 \sin^{-1} (c/h) + c(h^2 - c^2)^{1/2}] \quad [19]$$

for $h > c$.

Figure 5 shows the cross section $A_i(z)$ into which $A_o(z)$ is mapped. Its value is given by:

$$A_i(z) = 2[i_x^2 \sin^{-1} (i_y/i_x) + i_y (i_x^2 - i_y^2)^{1/2}] \quad [20]$$

for $i_x > i_y$, which results from $h > c$. i_x may be calculated from [17] since it is generated by h :

$$i_x(z) = r + 2R\bar{v} \left| \frac{1}{\bar{u}} - \frac{1}{u} \right| \quad [21]$$

whereas i_y , since it results from c , must be calculated from [18]:

$$i_y(z) = \bar{c}\bar{v}/u + R\bar{v} \left| \frac{1}{\bar{u}} - \frac{1}{u} \right| \quad [22]$$

The fraction of $A_1(z)$ that is intercepted by the detector can now be specified.

2.4 Fraction Intercepted by Circular Detector

$A_1(z)$ may, in general, cover the circular detector (of radius r) in four ways:

(a) $i_y > r$ and $i_x > r$ (Fig. 6(a)).

In this case the fraction of $A_1(z)$ that is received by the detector is:

$$F_1(z) = \pi r^2 / A_1(z) \quad [23]$$

$A_1(z)$ being given by eqs. 20 to 22.

(b) $i_y > r$; $i_x < r$.

UNCLASSIFIED

11

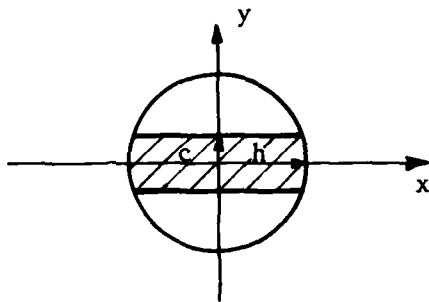


FIGURE 4 - Object space cross section: $A_o(z)$

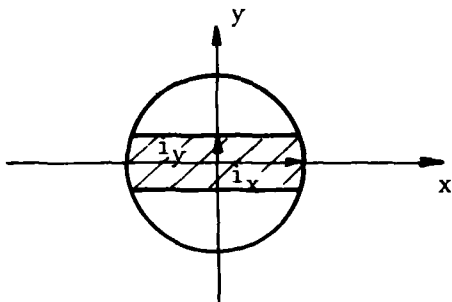


FIGURE 5 - Image space cross section: $A_i(z)$

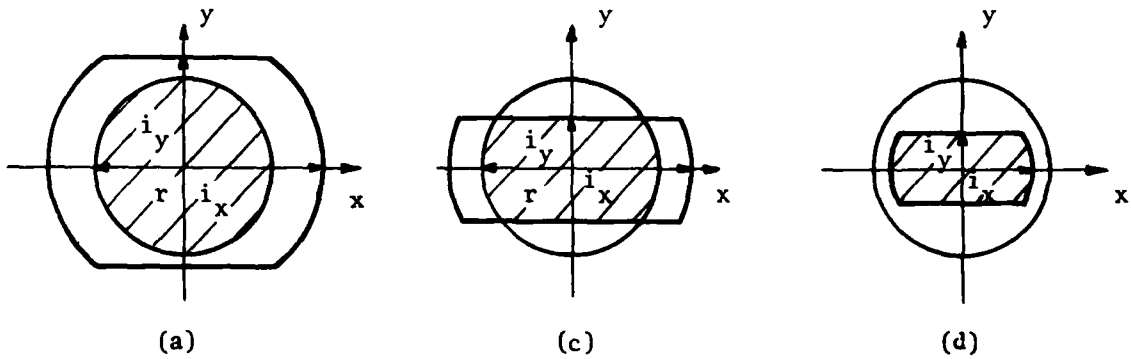


FIGURE 6 - Interception of $A_i(z)$ by a circular detector

This case does not occur because it implies $i_y > i_x$, which can not occur if h is chosen to be everywhere $> c$ (by adjustment of the distances \bar{v} and s).

(c) $i_x > r$; $i_y < r$ (Fig. 6 (c)).

The shaded area of Fig. 6(c) is

$$A_D(z) = 2[r^2 \sin^{-1} (i_y/r) + i_y (r^2 - i_y^2)^{1/2}], \quad [24]$$

and

$$F_1(z) = A_D(z)/A_1(z) \quad [25]$$

(d) $i_x < r$; $i_y < r$ (Fig. 6(d)).

In this case the entire area $A_1(z)$ is intercepted by the detector, and

$$F_1(z) = 1 \quad [26]$$

To summarize:

(1) at all points in z , we have defined an emitting area $A_e(z)$

(eq. 19) that can contribute to light intensity at the detector;

(2) through eqs. 23 to 26, we have obtained the fraction of this area that is mapped, by the lens, onto the detector; and

(3) it remains to define the fraction of light emitted by any point in $A_e(z)$ that arrives at the lens (essentially the

solid angle subtended to the lens), and hence by (1) and (2) above, the fraction of emitted light that arrives at the detector.

2.5 Fraction of Emitted Light Arriving at the Lens

This calculation is complicated by the fact that in the y-direction light emission is restricted by an opaque roof, and that to support a window, the cavity has a wall of thickness T where there is essentially no emitting gas.

Figure 7 shows a cross section in the yz-plane of the cavity/lens arrangement, indicating the window position and the angle subtended to the lens by a point on the viewing axis. The variable $Y(z)$ of Fig. 7 can be calculated from the geometry:

$$\tan\theta = c/(u-M) = Y/u \quad [27]$$

giving

$$Y(z) = uc/(u-M) ; (M = s - t) \quad [28]$$

Thus the area of a lens of radius R illuminated by an emitting point on the z-axis (shown in Fig. 8) is:

$$A_L(z) = 2[R^2 \sin^{-1}(Y/R) + Y(R^2 - Y^2)^{1/2}] \quad [29]$$

for $Y < R$, and

$$A_L(z) \equiv \pi R^2 \quad [30]$$

for $Y > R$.

UNCLASSIFIED

14

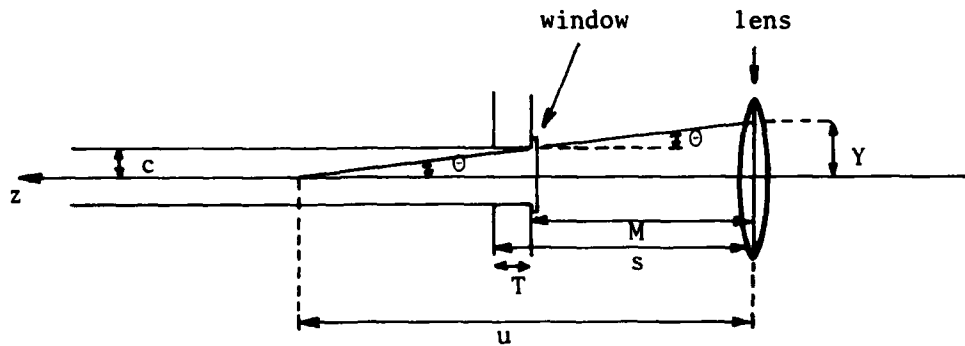
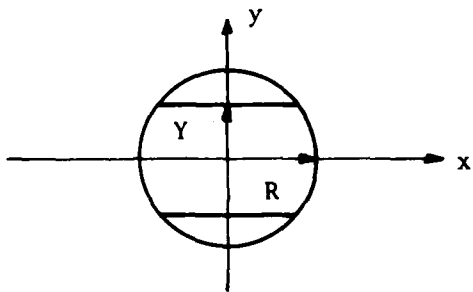


FIGURE 7 - Lens and cavity in the yz-plane

FIGURE 8 - Area of lens illuminated: $A_L(z)$

The case $Y > R$ occurs when the radiating point is close enough to the window to illuminate the entire lens area.

Thus the solid angle subtended to the lens (A_L/u^2) falls off more rapidly than simply $1/u^2$, since the cavity roof restricts the area of the lens that can intercept light; i.e. $A_L \rightarrow 0$ as z increases.

The fraction of light emitted by a point in $A_e(z)$ that arrives at the lens is given by:

$$F_L(z) = A_L(z)/4\pi u^2 \quad [31]$$

Equation 31 is exact only for points on the z -axis, but for small off-axis variations it is a very good approximation.

2.6 Relation Between Emitting Gas Concentration and Photon Flux at a Detector

If the radiative rate constant for spontaneous emission from the gas is k_s (s^{-1}), and the gas concentration is α (molecules cm^{-3}), then an infinitesimal volume element

$$\delta V = A_o(z) \delta z \quad (cm^3) \quad [32]$$

emits

$$\delta P = k_s \alpha A_o(z) \delta z \quad (\text{photons } s^{-1}) \quad [33]$$

in all directions.

Of these, $F_L(z) \cdot \delta P(z)$ arrive at the lens, and $F_1(z) \cdot F_L(z) \cdot \delta P(z)$ arrive at the detector.

Integrating over the extended volume (0 to L in z -space) gives the total number of photons per second arriving at the detector, P_{SL} , ignoring for the moment the transmittance of the window, the lens and a narrow-band interference filter. Thus:

$$P_{SL} = \int_0^L F_1(z) F_L(z) k_s \alpha A_o(z) dz \quad (\text{photons } s^{-1}) \quad [34]$$

or, from [31]

UNCLASSIFIED

16

$$P_{SL} = \frac{k_s \alpha}{4\pi} \int_0^L F_1(z) A_L(z) A_o(z) \cdot u^{-2} \cdot dz \quad [35]$$

The subscripts on P indicate spontaneous and lens respectively.

It is convenient to define a lens integral:

$$I_L \equiv \int_0^L F_1(z) A_L(z) A_o(z) \cdot u^{-2} \cdot dz \quad [36]$$

so that [35] can be written in a form that will be useful in future comparisons with results obtained for the viewing tube case. Equation 35 becomes:

$$P_{SL} = k_s \cdot \alpha \cdot I_L / 4\pi \quad [37]$$

2.7 Calculation of the Lens Integral: A Numerical Example

A FORTRAN program has been written to calculate the individual terms in the integrand of eq. 36 pointwise in z -space, and then perform the integral numerically using Simpson's rule. The precision of the result can always be verified by increasing the number of integration points. The following dimensions are required as input parameters:

r - active detector radius;
 R - lens radius;
 f - lens focal length;
 c - cavity y -dimension (Fig. 1);
 T - cavity wall thickness (Fig. 7);
 L - cavity z -dimension (Fig. 1);
 s - lens-to-source distance; and
 \bar{v} - lens-to-detector distance.

UNCLASSIFIED

17

Column one of Table I lists a particular set of values $\{q_i\}$ for these parameters, which correspond to an experiment using a gas flow containing excited oxygen ($O_2(a^1\Delta)$). The emission from this (at $1.27 \mu\text{m}$) was recorded with a Judson J-16 germanium detector through a narrow-band interference filter.

The value of the integral for this input set, $I_L\{q_i\}$, was found to converge to five significant figures (0.42401 cm^3) using 201 integration points.

Table I also gives an error analysis. The experimental uncertainties $\{\delta q_i\}$ in the measured dimensions $\{q_i\}$ are listed in column two, and the percentage uncertainties in column three. The total measurement uncertainty is thus about 8%. Column four shows the integral values obtained using a particular parameter at its maximum allowed value ($q_j + \delta q_j$) with all other parameters held at the values given in column one. Thus, column five shows the maximum percentage variation in I_L that can be introduced by the uncertainty in each of the input parameters. The total uncertainty in I_L is then about 9% due to the cumulative measurement error. Hence:

$$I_L = 0.4240 \pm 9\% \quad (\text{cm}^3) \quad [38]$$

2.8 Choice of \bar{v} and s : Maximization of I_L

In the absence of any other criteria, the lens and detector positions of Table I (s and \bar{v}) were chosen such that an object at the centre of the cavity ($z = L/2$), with a radius of about one and a half times the cavity height (i.e. $\bar{h} = 1.5 c$), would form an image at the detector with a radius equal to that of the detector (r). This ensures $h(z) > c$ for all z in 0 to L , as required by eq. 19.

UNCLASSIFIED

18

TABLE I

Input and error analysis in the calculation of I_L

Parameter value q_i	Uncertainty δq_i	$\% \delta q_i$	$I_L(q_j + \delta q_j)$	$\% \delta I_L$
r 0.412	0.001	0.2	0.42585	0.43
R 2.23	0.01	0.4	0.42586	0.44
f 6.35	0.05	0.8	0.41897	1.19
c 0.54	0.02	3.7	0.44325	4.54
T 1.21	0.01	0.8	0.42364	0.09
L 12.05	0.05	0.4	0.42486	0.20
S 12.9	0.10	0.8	0.42675	0.65
\bar{v} 9.5	0.10	1.0	0.41941	1.08

(q_i in centimeters; I_L - cm³)

However, it is possible to optimize s and \bar{v} by numerically maximizing the lens integral I_L of eq. 36, and hence by [37] ensuring that the photon flux at the detector is a maximum.

The numerical procedure is as follows: a particular s -value, s_j , is defined ($s_j > f$); I_L is calculated for a series of \bar{v} values converging to a maximum I_L (e.g. using the Newton-Raphson method) and hence also to an optimum \bar{v}_j . A pair (\bar{v}_j, s_j) can thus be defined for any $s > f$ that maximizes I_L , and by scanning through s an absolute maximum I_L and its associated optimum pair (\bar{v}, s) can be obtained.

Figures 9 and 10 show the results of such a calculation for the experimental setup described in Section 2.7. The absolute maximum of I_L occurs at:

UNCLASSIFIED
19

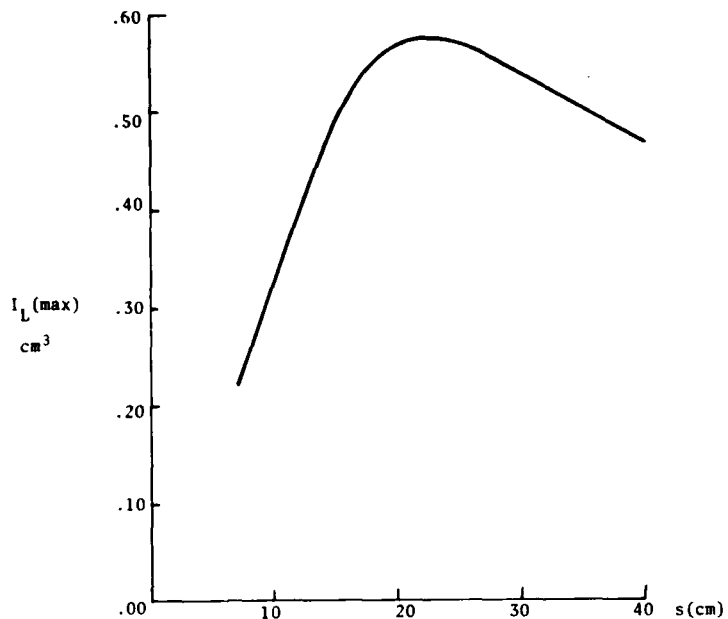


FIGURE 9 - Maximized I_L as a function of s

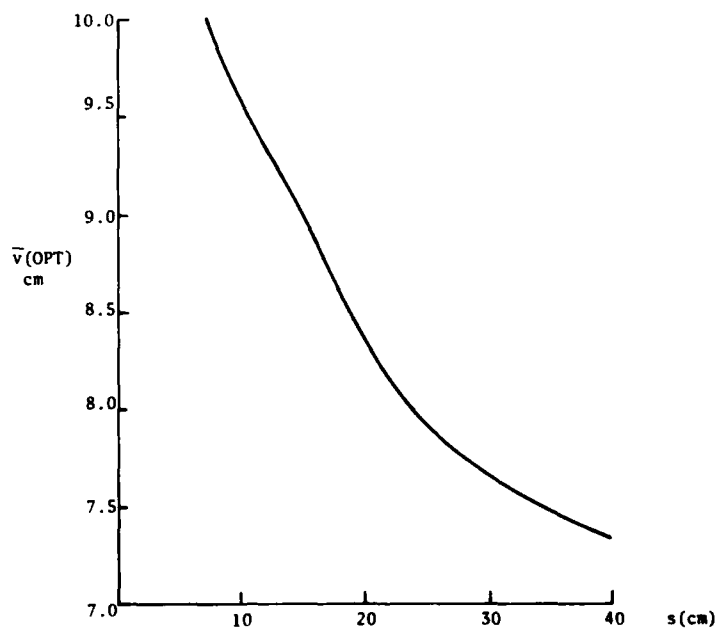


FIGURE 10 - Optimized \bar{v} as a function of s

$$s = 22.1 ; \bar{v} = 8.14 \text{ (cm)}$$

[39]

Equations 1 and 2 can be used to calculate the size (\bar{h}) and position (\bar{u}) of an object that is imaged exactly on the detector, for the optimized values of [39]. This yields:

$$\bar{u} = 28.9$$

$$\bar{z} = \bar{u} - s = 6.8$$

[40]

and $\bar{h} = 1.46$.

The nominal object position (\bar{z}) is thus displaced from the centre of the cavity (at $z = 6$) and the object radius (\bar{h}) is almost three times the cavity height.

These results are, of course, peculiar to the extended source considered here, which is restricted in two dimensions and unbounded in the third, and also to the lens and detector dimensions. However, the methods would be applicable to any extended source for which it is important to maximize a detector signal.

3.0 TUBE CASE

The equations derived in this chapter specify the number of photons per second arriving at a circular detector through a cylindrical tube placed between the extended source of Fig. 1 and the detector. The tube was blackened and baffled to minimize internal reflection. The purpose of this viewing tube is to define clearly the contributing volume of emitting gas.

Figure 11 shows the xz -plane of Fig. 1, indicating a tube of length K and radius R (exaggerated for clarity), and the volume of gas that can contribute to light intensity at the detector.

UNCLASSIFIED
21

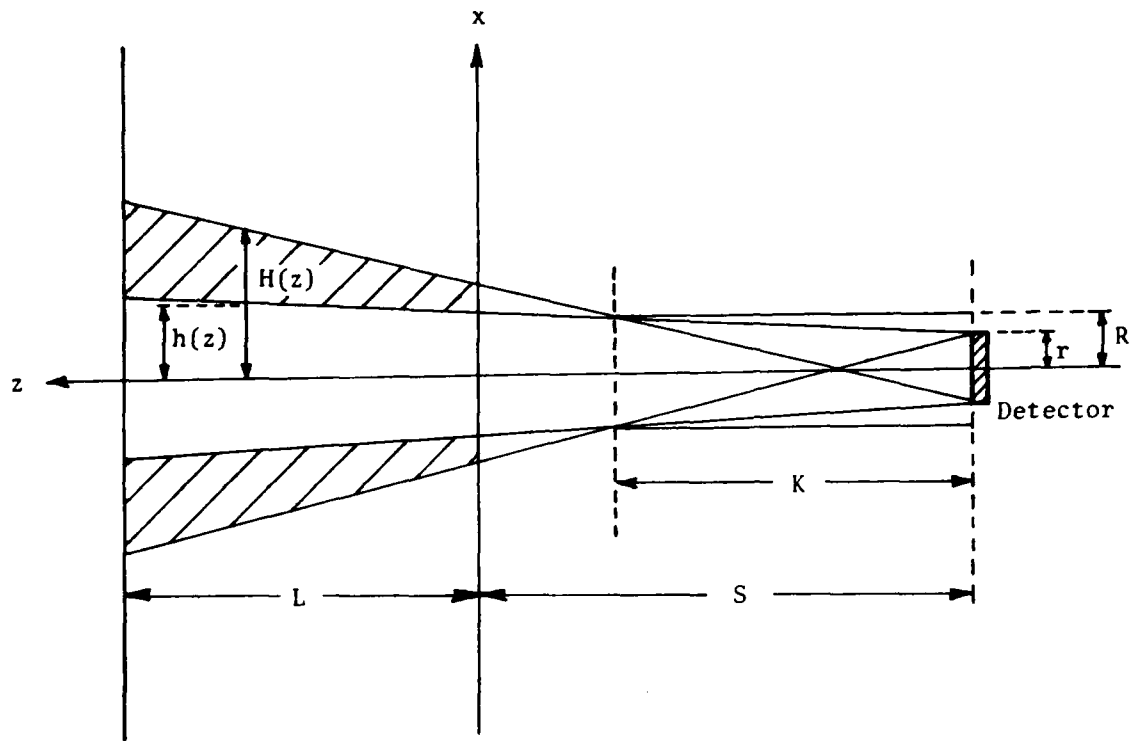


FIGURE 11 - Tube, detector and source in the xz -plane

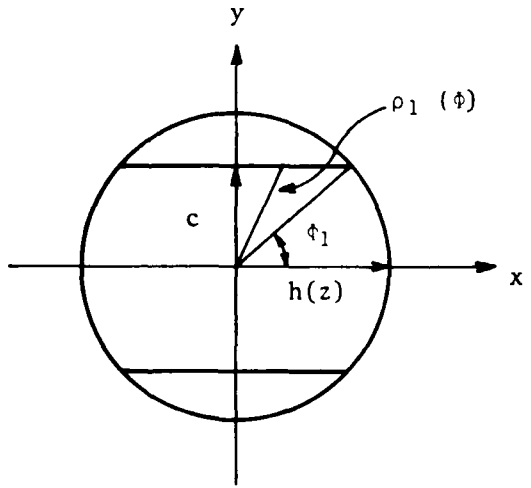


FIGURE 12 - Emitting cross section $A_1(z)$

Any point in the volume bounded by $h(z)$ (for $z = 0$ to L) in Fig. 11 may illuminate the entire detector surface. However, in the region $h(z)$ to $H(z)$ (shaded in Fig. 11), radiating molecules can only illuminate a fraction of the detector area. This fraction goes from 1 to 0 as x goes from h to H .

A first approximation, considering only the volume bounded by $h(z)$, will be presented, and subsequently the exact equations will be derived for the entire volume bounded by $H(z)$. It will be shown that the contribution from the shaded volume of Fig. 11 is not at all negligible; in fact it is of the same order of magnitude as the first approximation (for the tube length considered here). Clearly, it will go to zero as the tube length increases, but unfortunately so will the detector signal. In practice the tube length is therefore limited and the exact treatment must be used.

3.1 First Approximation: Detector Wholly Illuminated

From the geometry of Fig. 11:

$$h(z) = u(z) \cdot \frac{(R-r)}{K} + r \quad [41]$$

where, as in chapter 2,

$$u(z) = z + s \quad [42]$$

An emitting area, $A_1(z)$, in which any point can fully illuminate the detector, can thus be defined. Figure 12 shows this cross section, bounded by the cavity height (c) and the variable $h(z)$.

It is helpful in understanding the subsequent treatment of the shaded region of Fig. 11, to derive the area $A_1(z)$ in cylindrical polar coordinates:

$$A_1(z) = 4 \left\{ \int_0^{\Phi_1} \int_0^h \rho d\rho d\Phi + \int_{\Phi_1}^{\pi/2} \int_0^1 \rho d\rho d\Phi \right\} \quad [43]$$

where Φ_1 and ρ_1 , shown in Fig. 12, are given by

$$\Phi_1(z) = \sin^{-1}(c/h(z)) \quad [44]$$

and

$$\rho_1(\Phi) = c \operatorname{cosec} \Phi \quad [45]$$

Substitution of [44] and [45] into [43] leads to the familiar form (cf. eq. 19) for the area of a section of a circle:

$$A_1(z) = 2(h^2 \sin^{-1}(c/h) + c(h^2 - c^2)^{1/2}) ; (h > c) \quad [46a]$$

which may also be written:

$$A_1(z) = 2(h^2 \Phi_1 + c^2 \cot \Phi_1) \quad [46b]$$

$$(\text{if } c > h, A_1(z) = \pi h^2)$$

An infinitesimal volume element

$$\delta V = \rho \delta \rho \delta \Phi \delta z \quad [47]$$

centred at a position $u(z)$, containing α molecules cm^{-3} , would emit $k_s \alpha \delta V$ photons per second into a sphere of surface area $4\pi u^2$. If all points in δV can fully illuminate a detector of area

$$a = \pi r^2 \quad [48]$$

then the number of photons per second that arrive at the detector from δV is:

$$\delta P_1 = \frac{a}{4\pi u^2} k_s \alpha \delta V \quad [49]$$

Integrating over the volume bounded by $h(z)$ and the cavity length, and using [43] and [46]:

$$P_1 = \frac{a k_s}{4\pi} \int_0^L \frac{A_1(z)}{u^2} dz \quad [50]$$

which is valid provided $h(z)$ is small relative to $u(z)$. Using [48]:

$$P_1 = \frac{k_s \alpha r^2}{4} I_1 \quad [51]$$

which defines I_1 (cf. [50]).

P_1 is thus a first approximation to the number of photons s^{-1} arriving at the detector from the cavity, which ignores contributions from the region h to H of Fig. 11. In that region, an emitting molecule illuminates only a fraction of the detector area.

3.2 Inclusion of Boundary Region

Suppose that an infinitesimal volume element (eq. 47) contains molecules that irradiate a fractional area of the detector:

$$a(\rho, z) = F(\rho, z) \cdot \pi r^2 \quad [52]$$

$F(\rho, z)$ is the fraction of the total area (πr^2) that is irradiated by a molecule at (ρ, θ, z) , thus:

$$0 < F(\rho, z) < 1 \quad [53]$$

This fraction is independent of θ (cylindrical symmetry), but is dependent on ρ , and through the limits of ρ (h and H), on z .

UNCLASSIFIED

25

Equation 49 must now be replaced by:

$$\delta P_{ST} = \frac{a(\rho, z)}{4\pi u^2} \cdot k_s \delta V \quad [54]$$

Using [52] and integrating over the volume bounded by the cavity dimensions and $H(z)$ now,

$$P_{ST} = \frac{k_s \alpha r^2}{4} \int_V \frac{F(\rho, z)}{u^2} dV \quad [55]$$

and by analogy with [43]:

$$P_{ST} = \frac{k_s \alpha r^2}{4} \int_0^L \frac{dz}{u^2} \left\{ 4 \int_0^{\Phi_2} d\Phi \int_0^H F(\rho, z) \rho d\rho + \int_{\Phi_2}^{\pi/2} d\Phi \int_0^1 F(\rho, z) \rho d\rho \right\} \quad [56]$$

The subscripts on P indicate spontaneous and tube respectively.

The limits (Φ_2 and H) of the integrals in [56] now include the region h to H . From the geometry of Fig. 11:

$$H(z) = u(z) \cdot \frac{(R + r)}{K} - r \quad [57]$$

and by analogy with [44] (cf. Fig. 12 with h replaced by H , and Φ_1 by Φ_2):

$$\Phi_2(z) = \sin^{-1} (c/H(z)) \quad [58]$$

Now, if a weighted area $\bar{A}(z)$ is defined:

$$\bar{A}(z) \equiv 4 \left\{ \int_0^{\Phi_2} \int_0^H F(\rho, z) \rho d\rho d\Phi + \int_{\Phi_2}^{\pi/2} \int_0^1 F(\rho, z) \rho d\rho d\Phi \right\} \quad [59]$$

then [56] can be written in a form similar to [50] and [51]:

$$P_{ST} = \frac{k_s \alpha r^2}{4} \int_0^L \frac{\bar{A}(z)}{u^2} dz \equiv \frac{k_s \alpha r^2}{4} I_T \quad [60]$$

which defines I_T , a tube integral (cf. the lens integral case, eq. 37).

$\bar{A}(z)$ is a weighted area in that points in an area $A(z)$ (Fig. 12 with h replaced by H , and ϕ_1 by ϕ_2) are weighted according to the fraction of the detector they are capable of illuminating.

Equation 59 can be separated into the previously defined area $A_1(z)$ (eq. 43), and a weighted area $\bar{A}_2(z)$ associated with the region h to H in ρ -space. In $0 < \rho < h$, $F = 1$, thus [59] becomes:

$$\begin{aligned} \bar{A}(z) = 4 & \left\{ \int_0^{\phi_2} \int_h^H F \rho d\rho d\phi + \int_0^{\phi_2} \int_0^h \rho d\rho d\phi \right. \\ & \left. + \int_{\phi_1}^{\pi/2} \int_0^{\phi_2} \rho d\rho d\phi + \int_{\phi_2}^{\phi_1} \int_0^{\phi_1} \frac{\rho}{h} F \rho d\rho d\phi + \int_{\phi_2}^{\phi_1} \int_0^h \rho d\rho d\phi \right\} \quad [61] \end{aligned}$$

which, by comparison with [43] can be seen to yield:

$$\bar{A}(z) = 4 \left[\phi_2(z) \int_h^H F(\rho, z) \rho d\rho + \int_{\phi_2}^{\phi_1} \int_0^{\phi_1} \frac{\rho}{h} F(\rho, z) \rho d\rho d\phi \right] + A_1(z) \quad [62]$$

or

$$\bar{A}(z) \equiv \bar{A}_2(z) + A_1(z) \quad [63]$$

defining $\bar{A}_2(z)$.

Thus it is possible to compare the effect of including the shaded area of Fig. 1 with the first approximation given by eqs. 50, 51. Equation 60 with [63] gives:

UNCLASSIFIED

27

$$P_{ST} = \frac{k \alpha r^2}{4} \{ I_1 + \int_0^L \frac{\bar{A}_2(z)}{u^2} dz \} \quad [64]$$

i.e.

$$P_{ST} = \frac{k \alpha r^2}{4} \{ I_1 + I_2 \} \quad [65]$$

where

$$I_2 \equiv \int_0^L \frac{\bar{A}_2(z)}{u^2} . dz \quad [66]$$

It only remains to define $F(\rho, z)$, the fraction of the detector area illuminated by a molecule at ρ between $h(z)$ and $H(z)$. This is algebraically complicated, and is treated in detail in Appendix A. Conceptually, it is only necessary to know that an explicit algebraic form exists for $F(\rho, z)$ in terms of tube and detector dimensions and the distance s , which satisfies [53], so that the integrals in [62] can be calculated numerically.

It is convenient for such a calculation, to write F in the form:

$$F(\rho, z) = 1 - G(\rho, z) \quad ; \quad (h < \rho < H; 0 < z < L) \quad [67]$$

where G varies from 0 to 1 as ρ goes from h to H .

Equation 62 may then be expressed, after some calculus and algebra, as:

$$\begin{aligned} \bar{A}(z) = 4\{\Phi_2(z)[\frac{1}{2}(H^2 - h^2) - \int_h^H G(\rho, z)\rho d\rho] - \frac{1}{2}h^2(\Phi_1 - \Phi_2) \\ - \frac{\Phi_1}{\Phi_2} \int_h^H G(\rho, z)\rho d\rho + \frac{c}{2}[(H^2 - c^2)^{\frac{1}{2}} - (h^2 - c^2)^{\frac{1}{2}}]\} + A_1(z) \quad [68] \end{aligned}$$

Defining the two integrals in [68] to be I_p and $I_{p\phi}$, and then rearranging:

$$\bar{A}(z) = 4\{\frac{1}{2}[\phi_2 H^2 - \phi_1 h^2] - \phi_2 I_p - I_{p\phi} + \frac{c}{2}(\cot\phi_2 - \cot\phi_1)\} + A_1(z) \quad [69]$$

$A_1(z)$ can thus be eliminated by using [46b]:

$$\bar{A}(z) = 4[\phi_2(\frac{1}{2}H^2 - I_p) + \frac{1}{2}c^2 \cot\phi_2 - I_{p\phi}] \quad [70]$$

Equation 70 is a rather simple form for directly calculating the weighted area $\bar{A}(z)$ needed for the tube integral I_T of eq. 60. The integrals in p - and ϕ -space are:

$$I_p(z) \equiv \int_h^H G(p, z) p dp \quad [71]$$

$$I_{p\phi}(z) \equiv \int_{\phi_2}^{\phi_1} d\phi \left[\int_h^H G(p, z) p dp \right] \quad [72]$$

If $c > h$, eq. 70 is still valid, but with ϕ_1 replaced by $\pi/2$ in [72] for $I_{p\phi}$.

3.3 Calculation of the Tube Integral: A Numerical Example

A FORTRAN program calculates both the first approximation integral I_1 (eq. 51) and the accurate form I_T (eq. 60) using [46] and [70] for the numerators in the integrands. The z -space integrations are performed numerically using Simpson's rule. For I_T , at each point in z -space a p -space integral [71] is performed for $I_p(z)$, and a double integral is performed for $I_{p\phi}(z)$ (eq. 72): at each point in ϕ -space a p -space integral must be calculated since the upper limit of the p -

integral is Φ -dependent. All the functions vary smoothly, and a rapid convergence to five significant figures is obtained with only 25 points for each numerical integration.

The required input dimensions are:

L - cavity z-dimension (Figs. 1 and 11)

c - cavity y-dimension (Fig. 1)

s - detector-to-source distance (Fig. 11)

R - tube radius (Fig. 11)

r - detector radius (Fig. 11)

K - tube length (Fig. 11)

Table II lists a set of experimental values for these parameters, together with an error analysis as in Table I, corresponding to an experiment using a gas flow of excited oxygen as described in Section 2.7.

The total measurement error for this input is about 8%, which is shown in Table II to give a comparable total uncertainty in the tube integral I_T . Thus:

$$I_T = 0.4135 \text{ E-01} \pm 8\% \text{ (cm.)} \quad [73]$$

The first approximation I_1 was 0.2160E-01 , which is only 52% of I_T . Thus the contribution to the photon flux at the detector from the boundary region (h to H , the shaded region of Fig. 11) is of a similar magnitude to that from the region in which all molecules can fully illuminate the detector. In general, the full integral must be calculated.

TABLE II
Input and error analysis in the calculation of I_T

Parameter value q_i	Uncertainty δq_i	$\% \delta q_i$	$10x I_T(q_j + \delta q_j)$	$\% \delta I_T$
L 12.05	0.05	0.4	0.41484	0.33
c 0.54	0.02	3.7	0.42648	3.14
s 18.2	0.20	1.1	0.41028	0.77
R 0.49	0.01	2.0	0.42371	2.47
r 0.412	0.001	0.2	0.41341	0.02
K 11.9	0.1	0.8	0.40973	0.91

(all values in centimeters)

4.0 LENS/TUBE RATIO: THEORY AND EXPERIMENT

For the cavity of Fig. 1 and a lens-detector setup as in Fig. 2, eq. 37 gave the number of photons per second arriving at the detector. This must be modified to include transmission factors for the window (wtf), lens (ltf) and narrow-band interference filter (ftf), thus:

$$P_{SL} = (wtf) \cdot (ltf) \cdot (ftf) \cdot k_s \alpha I_L / 4\pi. \quad [74]$$

For example, a quartz lens has 92% transmission at $1.27 \mu\text{m}$, in which case $ltf = 0.92$.

For the same cavity, but with a tube-detector setup (Fig. 11), the photon flux at the detector was given by [60]. Again modified to include transmission factors (no lens) this becomes:

$$P_{ST} = (wtf) \cdot (ftf) k_s \alpha I_T \cdot r^2 / 4 \quad [75]$$

Thus for a given gas emitting at a rate k_s , with a fixed concentration α , viewed with the same detector through the same filter, the ratio of the lens and tube arrangements is:

UNCLASSIFIED

31

$$\frac{P_{SL}}{P_{ST}} = \frac{(1tf)}{\pi r^2} \cdot \frac{I_L}{I_T} \quad [76]$$

Experimentally, the detector signals are measured as voltages (V_L and V_T for lens and tube cases respectively), which are related to photons s^{-1} by a calibration constant Γ , thus:

$$P_{SL} = \Gamma V_L \quad ; \quad P_{ST} = \Gamma V_T \quad [77]$$

Hence an experimental value for the ratio of lens to tube integrals can be obtained from [77] and [76]:

$$\left. \frac{I_L}{I_T} \right|_{expt.} = \frac{\pi r^2}{(1tf)} \cdot \frac{V_L}{V_T} \quad [78]$$

For the excited oxygen emission experimental setups considered in Sections 2.7 and 3.3, theoretical values for I_L and I_T were obtained (eqs. 38 and 73), giving the theoretical ratio:

$$\left. \frac{I_L}{I_T} \right|_{theory} = \frac{0.4240}{0.04135} = 10.3 \quad [79]$$

Table III shows the results from a series of experiments in which different total oxygen pressures were used in the cavity, i.e. different values of α , the emitting O_2 concentration. The corresponding detector signals, measured using the aforementioned tube and lens arrangements, and their ratios are given. The ratio obtained at any fixed pressure should be independent of the pressure. The table shows that this is the case since no ratio deviates by more than 2% from the average (18.83).

UNCLASSIFIED

32

TABLE III

Detector readings for several gas pressures

Pressure (torr)	V_L (μ V)	V_T (μ V)	V_L/V_T
1	185	9.7	19.1
2	327	17.7	18.5
3	443	23.7	18.7
4	535	28.0	19.1

The experimental value for the ratio $I_L:I_T$ is then given by [78], with $r = 0.412$ and $l_{tf} = 0.92$,

$$\left. \frac{I_L}{I_T} \right|_{\text{expt.}} = \frac{\pi(0.412)^2}{0.92} (18.83) = 10.9 \quad [80]$$

The difference between the theoretical and experimental ratios is less than 6%, which is well within the uncertainty introduced into the theoretical ratio (about 17%) by uncertainties in the measured dimensions.

The absolute concentration α of an emitting gas in the cavity of Fig. 1 is related to the measured voltage from a calibrated detector:

a) in the lens case using eqs. 74 and 77,

$$\alpha = 4\pi I V_L / (\text{wtf})(\text{lrf})(\text{tf}) k_s I_L ; \quad [81]$$

b) in the tube case using [75] and [77],

$$\alpha = 4\pi I V_T / (\text{wtf})(\text{tf}) k_s I_T r^2 . \quad [82]$$

UNCLASSIFIED

33

The integrals I_L and I_T are calculated from physical dimensions only (Chapters 2 and 3), and Γ is the detector calibration constant. The integrals may be computed to a high precision, but the values are only as accurate as the total dimension measurement error, which is typically less than 10%. The accuracy of the calculated concentration is also dependent upon the accuracy of the known emission rate (k_g) which is about 10% in the excited oxygen case, and the detector calibration (< 10%). The transmission factors and voltage measurements can be quite accurately measured (about 1%).

An overall concentration measurement that is accurate to within about 30% can therefore be expected.

Absolute concentrations of a particular excited species, $O_2(a^1\Delta)$ in the gas flow from a chemical generator, have been estimated by observing two entirely different emissions arising from this molecule. The first of these emissions (at 1268 nm), the direct spontaneous transition to the ground state, was observed with a germanium detector/filter combination using both tube and lens arrangements, and gave rise to the voltages listed in Table III. From these, partial pressures of $O_2(a^1\Delta)$ were calculated in the range from 0.22 to 0.63 torr as the total O_2 pressure varied between 1 and 4 torr. Observation of the second emission (the red "dimole" emission at 634 nm) using a silicon detector and appropriate filter, led to estimated $O_2(a^1\Delta)$ partial pressures between 0.27 and 0.69 torr over the same total pressure range.

Agreement between the estimates from the two emissions is within the anticipated 30% accuracy, and the average of the calculated percentages of $O_2(a^1\Delta)$ in the flow (varying between 25 and 17% over the 1 to 4 torr total O_2 pressure range) is of the expected magnitude for chemically generated singlet delta oxygen (Ref. 7) in the flow system employed in these experiments.

UNCLASSIFIED

34

5.0 CONCLUSIONS

The concentration of a photon-emitting gas contained in an extended source can be estimated using a calibrated detector, narrow-band interference filter, and either a lens or a viewing tube to define the contributing gas volume.

The close agreement between theory and experiment for the ratio of intensities at a detector for the two cases gives us confidence in the methods and formulae developed in this report. The final two equations could, of course, both be in error by the same multiplicative constant. Though specifically applied to a source of rectangular cross section, the methods can be modified for any extended source without difficulty, and the lens treatment provides a method for optimizing the light intensity at a detector from such a general source.

6.0 ACKNOWLEDGEMENTS

The author thanks Dr. T. Jacobson for providing many useful concepts and constructive criticism of this work.

UNCLASSIFIED

35

7.0 REFERENCES

1. Badger, R.M., Wright, A.C. and Whitlock, R.F., J. Chem. Phys., Vol. 43, p. 4345, 1965.
2. Tennyson, P.H., Fontijn, A. and Clyne, M.A.A., Chem. Phys., Vol. 62, p. 171, 1981.
3. Weiner, M.M., J.O.S.A., Vol. 54, p. 1109, 1964.
4. Sommerfeld, A., "Optics", Academic Press Inc., New York, 1954.
5. Nielsen, J.R., J.O.S.A., Vol. 37, p. 494, 1947.
6. Nielsen, J.R., J.O.S.A., Vol. 20, p. 701, 1930.
7. McDermott, W.E., Pchelkin, N.R., Benard, D.J., and Bousek, R.R., Appl. Phys. Lett., Vol. 32, p. 469, 1978.

APPENDIX AFractional Area of a Circular Detector Illuminated
Through a Cylindrical Tube by a Radiating
Off-Axis Molecule

Referring to Fig. A-1, consider first an on-axis point that fully illuminates the end of the tube farthest from the detector. The projection of this circle onto the plane of the detector by the rays indicated in the figure has a radius R_p given by:

$$\tan \theta = R/(u-K) = R_p/u \quad [A-1]$$

Thus,

$$R_p(z) = Ru/(u-K) \quad [A-2]$$

As the point moves off-axis and into the region where $h < \rho < H$, this projected circle essentially moves across the detector. There will be some distortion from a circle, and R_p will increase slightly as ρ becomes large. However, for small off-axis displacements the projection can be considered to be a displaced circle of radius R_p . It would not be difficult to write the exact elliptical equation for the projected curve, but the deviation from this is negligible here because: a) we are concerned only with the area of intersection of the detector circle and the projection, the deviation from the circular curvature of which is minimal in the small arc covering the detector; and b) at the extreme value $\rho = H$, where the deviation from a circle is the greatest, this is also where the contribution to the integral I_T is the smallest because the fractional area illuminated is close to zero.

UNCLASSIFIED

37

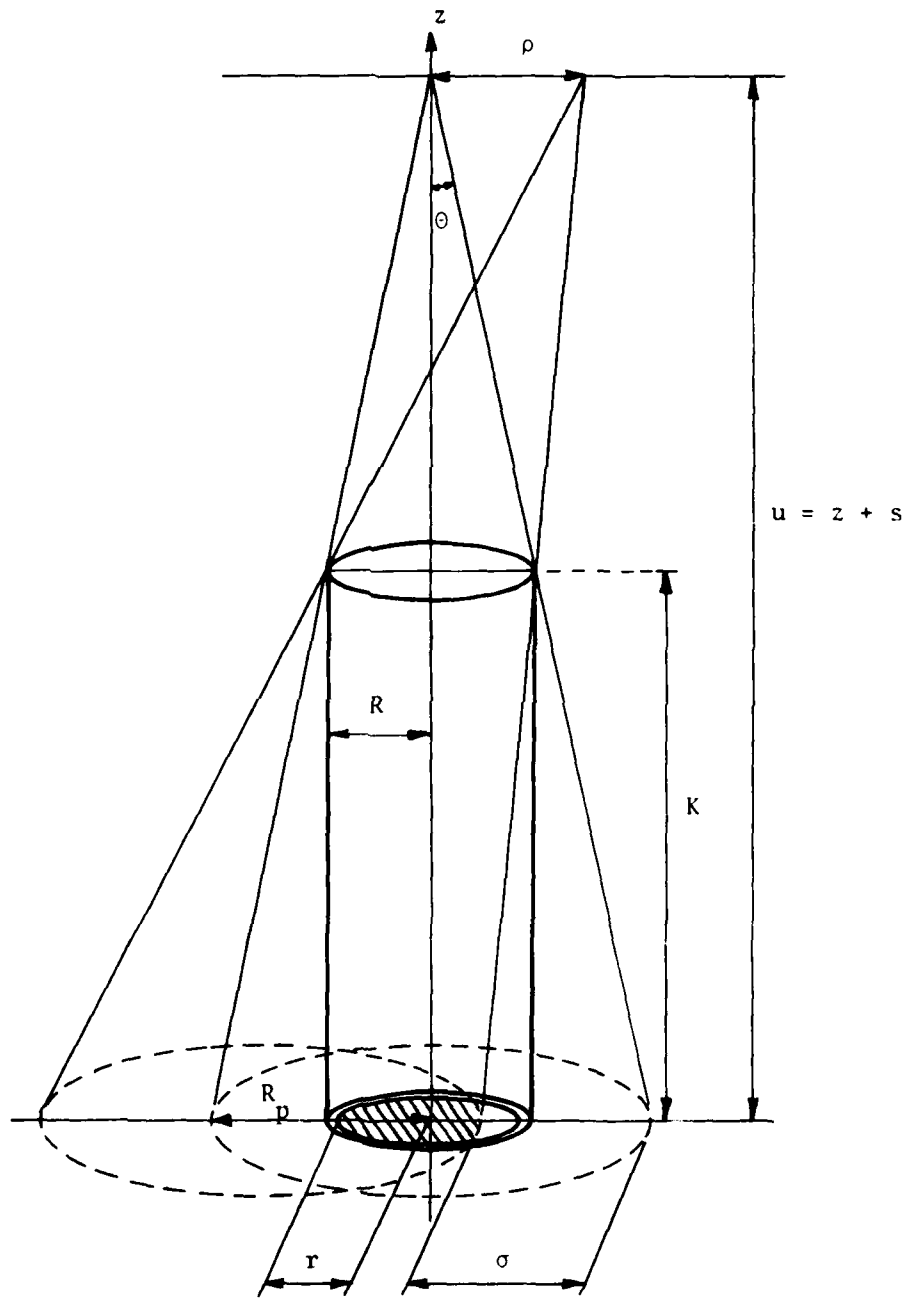


FIGURE A-1 - Illumination of a circular detector through a cylindrical tube

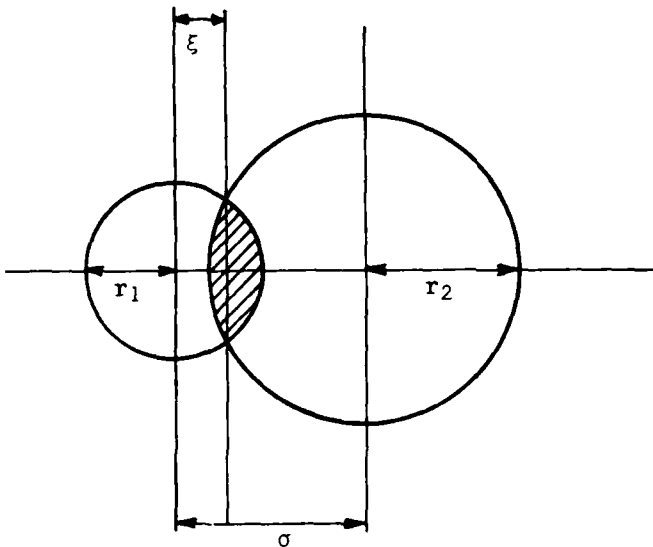


FIGURE A-2 - Area of intersection of two circles

Now, the area of intersection of two circles (Fig. A-2) of radii $r_1 < r_2$ is given by:

$$A_I = \frac{\pi}{2} r_2^2 - (\sigma - \xi) [r_2^2 - (\sigma - \xi)^2]^{\frac{1}{2}} - r_2^2 \sin^{-1} \left(\frac{\sigma - \xi}{r_2} \right) + \frac{\pi}{2} r_1^2 - \xi (r_1^2 - \xi^2)^{\frac{1}{2}} - r_1^2 \sin^{-1} \left(\frac{\xi}{r_1} \right) \quad [A-3]$$

where σ is the distance between the centres of the two circles, and

$$\xi = [\sigma^2 - (r_2^2 - r_1^2)]/2\sigma \quad [A-4]$$

In the case considered here,

$$r_2 \equiv R_p, \quad r_1 \equiv r \quad [A-5]$$

and σ may be calculated from the geometry of Fig. A-1:

$$\sigma(z, \rho) = K\rho / (u - K) \quad [A-6]$$

Hence $F(\rho, z)$, the fractional area of the detector illuminated is:

$$\begin{aligned} F(\rho, z) = A_1 / \pi r^2 &= \frac{1}{2} (R_p / r)^2 - \left\{ (\sigma - \xi) \left[R_p^2 - (\sigma - \xi)^2 \right]^{\frac{1}{2}} + R_p^2 \sin^{-1} \left(\frac{\sigma - \xi}{R_p} \right) \right\} / \pi r^2 \\ &+ \frac{1}{2} - \xi (r^2 - \xi^2)^{\frac{1}{2}} / \pi r^2 - \left[\sin^{-1} \left(\frac{\xi}{r} \right) \right] / \pi \quad [A-7] \end{aligned}$$

Equation A-7 may be rearranged to give a form (cf. eq. 67):

$$F(\rho, z) = 1 - G(\rho, z) \quad [A-8]$$

where

$$G(\rho, z) = [T(\rho, z) / \pi - (R_p^2 - r^2) / 2] / r^2 \quad [A-9]$$

and

$$\begin{aligned} T(\rho, z) &= (\sigma - \xi) \left[R_p^2 - (\sigma - \xi)^2 \right]^{\frac{1}{2}} + R_p^2 \sin^{-1} \left(\frac{\sigma - \xi}{R_p} \right) \\ &+ \xi (r^2 - \xi^2)^{\frac{1}{2}} + r^2 \sin^{-1} \left(\frac{\xi}{r} \right) \quad [A-10] \end{aligned}$$

Thus, equations A-8 to A-10, together with [A-6] for σ , [A-4] for ξ , and [A-2] for R_p , define the fractional area required.

CRDV R-4290/83 (NON CLASSIFIÉ)

Bureau - Recherche et Développement, MDN, Canada.
CRDV, C.P. 8800, Courcellette, Qué. G0A 1R0

"Evaluation de la concentration d'un gaz émettant dans une source étendue" par S. Barton

Selon l'optique géométrique, on a dérivé des équations qui reliaient le flux de photons atteignant un détecteur à la concentration d'un gaz émettant dans une source étendue dont la coupe transversale est rectangulaire. Deux arrangements optiques sont considérés. Puisque le rapport des signaux expérimentaux pour ces deux cas tout à fait différents est en accord avec celui prédit théoriquement, les méthodes sont validées.

Une méthode est décrite afin de maximiser le signal d'un détecteur, pour une lentille donnée. Cette méthode peut être appliquée dans le cas d'une source étendue ayant une coupe transversale arbitraire.

CRDV R-4290/83 (NON CLASSIFIÉ)

Bureau - Recherche et Développement, MDN, Canada.
CRDV, C.P. 8800, Courcellette, Qué. G0A 1R0

"Evaluation de la concentration d'un gaz émettant dans une source étendue" par S. Barton

Selon l'optique géométrique, on a dérivé des équations qui reliaient le flux de photons atteignant un détecteur à la concentration d'un gaz émettant dans une source étendue dont la coupe transversale est rectangulaire. Deux arrangements optiques sont considérés. Puisque le rapport des signaux expérimentaux pour ces deux cas tout à fait différents est en accord avec celui prédit théoriquement, les méthodes sont validées.

Une méthode est décrite afin de maximiser le signal d'un détecteur, pour une lentille donnée. Cette méthode peut être appliquée dans le cas d'une source étendue ayant une coupe transversale arbitraire.

CRDV R-4290/83 (NON CLASSIFIÉ)

Bureau - Recherche et Développement, MDN, Canada.
CRDV, C.P. 8800, Courcellette, Qué. G0A 1R0

"Evaluation de la concentration d'un gaz émettant dans une source étendue" par S. Barton

Selon l'optique géométrique, on a dérivé des équations qui reliaient le flux de photons atteignant un détecteur à la concentration d'un gaz émettant dans une source étendue dont la coupe transversale est rectangulaire. Deux arrangements optiques sont considérés. Puisque le rapport des signaux expérimentaux pour ces deux cas tout à fait différents est en accord avec celui prédit théoriquement, les méthodes sont validées.

Une méthode est décrite afin de maximiser le signal d'un détecteur, pour une lentille donnée. Cette méthode peut être appliquée dans le cas d'une source étendue ayant une coupe transversale arbitraire.

CRDV R-4290/83 (NON CLASSIFIÉ)

Bureau - Recherche et Développement, MDN, Canada.
CRDV, C.P. 8800, Courcellette, Qué. G0A 1R0

"Evaluation de la concentration d'un gaz émettant dans une source étendue" par S. Barton

Selon l'optique géométrique, on a dérivé des équations qui reliaient le flux de photons atteignant un détecteur à la concentration d'un gaz émettant dans une source étendue dont la coupe transversale est rectangulaire. Deux arrangements optiques sont considérés. Puisque le rapport des signaux expérimentaux pour ces deux cas tout à fait différents est en accord avec celui prédit théoriquement, les méthodes sont validées.

Une méthode est décrite afin de maximiser le signal d'un détecteur, pour une lentille donnée. Cette méthode peut être appliquée dans le cas d'une source étendue ayant une coupe transversale arbitraire.

DREV R-4290/83 (UNCLASSIFIED)

Research and Development Branch, DND, Canada.

DREV, P.O. Box 8800, Courclette, Que. G0A 1R0

"Estimation of the Concentration of a Photon-Emitting Gas in an Extended Source" by S. Barton

Equations are derived, within the framework of geometrical optics, that relate the photon flux at a detector to the concentration of an emitting gas contained in an extended source of rectangular cross section, for two optical arrangements that have been used experimentally. Since the ratio of the experimental detector signals for the two quite dissimilar cases is in agreement with that predicted theoretically, the methods are validated.

A method is described for maximizing the signal at the detector, using a given lens, which may be applied to an extended source of general cross section.

DREV R-4290/83 (UNCLASSIFIED)

Research and Development Branch, DND, Canada.

DREV, P.O. Box 8800, Courclette, Que. G0A 1R0

"Estimation of the Concentration of a Photon-Emitting Gas in an Extended Source" by S. Barton

Equations are derived, within the framework of geometrical optics, that relate the photon flux at a detector to the concentration of an emitting gas contained in an extended source of rectangular cross section, for two optical arrangements that have been used experimentally. Since the ratio of the experimental detector signals for the two quite dissimilar cases is in agreement with that predicted theoretically, the methods are validated.

A method is described for maximizing the signal at the detector, using a given lens, which may be applied to an extended source of general cross section.

DREV R-4290/83 (UNCLASSIFIED)

Research and Development Branch, DND, Canada.

DREV, P.O. Box 8800, Courclette, Que. G0A 1R0

"Estimation of the Concentration of a Photon-Emitting Gas in an Extended Source" by S. Barton

Equations are derived, within the framework of geometrical optics, that relate the photon flux at a detector to the concentration of an emitting gas contained in an extended source of rectangular cross section, for two optical arrangements that have been used experimentally. Since the ratio of the experimental detector signals for the two quite dissimilar cases is in agreement with that predicted theoretically, the methods are validated.

A method is described for maximizing the signal at the detector, using a given lens, which may be applied to an extended source of general cross section.

DREV R-4290/83 (UNCLASSIFIED)

Research and Development Branch, DND, Canada.

DREV, P.O. Box 8800, Courclette, Que. G0A 1R0

"Estimation of the Concentration of a Photon-Emitting Gas in an Extended Source" by S. Barton

Equations are derived, within the framework of geometrical optics, that relate the photon flux at a detector to the concentration of an emitting gas contained in an extended source of rectangular cross section, for two optical arrangements that have been used experimentally. Since the ratio of the experimental detector signals for the two quite dissimilar cases is in agreement with that predicted theoretically, the methods are validated.

A method is described for maximizing the signal at the detector, using a given lens, which may be applied to an extended source of general cross section.

